



## ORIGINAL ARTICLE

# Optimization of process parameters of friction stir welded joint of dissimilar aluminum alloy by response surface methodology

Prashant Kumar, Sunil Kadiyan, Rajesh Kumar

Department of Mechanical Engineering, Ganga Technical Campus, Bahadurgarh, M. D. University, Rohtak, Haryana, India

### Article Information

Received: 19 May 2022  
Revised: 30 June 2022  
Accepted: 17 July 2022  
Available online: 28 July 2022

### Keywords:

Tensile strength;  
Micro hardness;  
Residual Stress;  
Optimization;  
Friction stir welding;

### Abstract

Aluminum and its alloys are lightweight, affordable, high-strength materials that find extensive use in shipbuilding, automotive, construction, aerospace, and other industrial fields. They are also resistant to corrosion. There is a requirement to join components manufactured of various aluminum alloys, namely AA6061 and AA7475, in applications like the aerospace, marine, and automotive sectors. Friction stir welding (FSW) is utilized in this study to join dissimilar plates consisting of aluminum alloys 6061 and 7475. On the tensile strength and percentage elongation of the welded joints, the impact of changing the tool pin profile, tool rotation speed, tool feed rate, and tool tilt angle has been studied. The empirical relationship between the output responses and input parameters was developed, and the perceived optimal values of UTS, % strain and micro hardness at SZ were 205.23 MPa, 16.43 %, and 81.05 HV, respectively. The optimal TS, TRS, and tilt angle values were 87.42 mm-min<sup>-1</sup>, 783.92 rev/m, and 0.48°, respectively. Due to DRX, the microstructure in the weld SZ was characterized by a very fine grain structure. Because of the decreased hardness, the grain sizes in HAZ and TMAZ are virtually comparable, and they discovered coarse grain structure and uneven temperature distribution in that region. When the TRS and TS increase, the grain size decreases in the SZ.

©2022 ijrei.com. All rights reserved

## 1. Introduction

Automobile and aircraft industries focused on weight reduction factors to improve fuel economy and reduce environmental pollution. Aluminum alloys attracted all these industries because of their excellent strength-to-weight ratio and damage tolerance. The joining of dissimilar aluminum alloys has a lot of scope in the automotive, aircraft and shipbuilding industries. The first challenge within the fusion welding of aluminum alloy is weld cracking due to solidification [1]. Investigating how welding factors affect the structure and characteristics of the nugget zone in aluminum alloys, it was revealed that there is an ideal rotating speed for a given traverse speed that produces the nugget zone's best strength and ductility. The rotational speed must also grow as the traverse speed does. The grain size and hardness of the

welds differ significantly from top to bottom for a given traverse speed [2]. Because the material flow during friction stir welding is primarily controlled by both advancing and rotating speeds, the material flow in the weld zone is not evenly distributed along the weld line [3]. Researchers and practitioners are welding many combinations of dissimilar alloys and materials due to their requirements in varied service conditions [4, 5]. AA6XXX and AA7XXX Al alloys are two series of the most widely used structural materials in the automotive, rail transportation, and aerospace industries [6]. Alloy 6061 Al is the most used of the 6XXX series aluminum alloys, possesses superior weldability compared to other heat treatable alloys, and is the most popular aluminum alloy extrusion [7-11]. The medium-strength (Al-Mg-Si) aluminum alloys such as AA6061 are highly suited for applications in marine structures, pipelines, and storage tanks

[12]. One of the strongest aluminum alloys used in today's manufacturing industry is AA7075 (Al-Zn-Mg-Cu). AA7075 has high strength compared to its weight and natural ageing characteristics, making it attractive for aerospace structural applications.

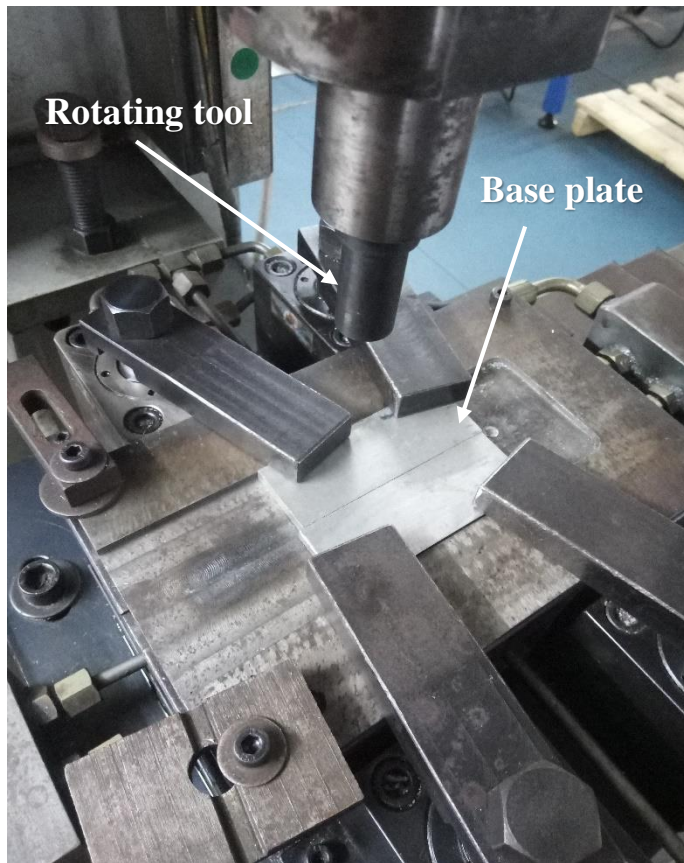


Figure 1: Friction Stir Welding

Defect-free welds with good mechanical properties have been made in various aluminium alloys, even those previously thought to be not weldable. Friction stir welds will not encounter problems like porosity, alloy segregation and hot cracking, and welds are produced with a good surface finish, and thus no post weld cleaning is required [13]. The process steps are clamping and positioning of workpiece and tool, tool plunging into the workpiece, tool traversing along the joint line and tool removal after completion of welding. The FSW tool consists of three parts: shank, shoulder and pin. Shank is used for holding purposes, and the shoulder and pin generate frictional heat on the workpiece. The shoulder is mainly responsible for generating heat and containing the plasticized material in the weld zone. At the same time, the pin mixes the material of the components to be welded, thus creating a joint [14]. In aircraft and automotive structures, friction stir welded lap joints have been widely used with the aim of replacing riveted lap joints by using aluminium alloys from the 2XXX to 7XXX series. Rivet holes are often potential sites for crack initiation or corrosion problems; moreover, eliminating fasteners leads to considerable weight and cost savings. As the FSW joining process is accomplished by material flow below the melting temperature, many joint defects

caused by joint melting, such as porosity, grain boundary cracks and alloys segregation, can be eliminated or adequately reduced. These process specialities have made FSW practical for joining dissimilar alloys [15]. Hence we used the FSW process for joining aluminium alloys AA 6061 and AA 7075. The New welding approach has been introduced to improve the welding quality of TIG welded joint, the influence of friction stir processing on TIG welded joint have been analyzed and they observed mechanical properties and heat transfer of TIG+FSP welded joint. The mechanical properties of TIG+FSP welded joint were observed better than TIG welded joints. [16-22]. It was evident that welding processes have multiple responses. Various multi-objective optimization approaches, such as statistical techniques and evolutionary algorithms, provide good results to optimize a process with multiple objectives. In the case of statistical methods, Kasman [23] combined Taguchi with grey relational analysis to optimize a multi-response FSW of AA6082 and AA5754 Al alloys. Rajakumar and Balasubramanian [24] employed the desirability approach to finding the optimal conditions to maximize UST and minimize the corrosion rate for FSW AA1100 Al alloys. In the case of metaheuristic algorithms, Teimouri and Baseri [25] developed a fuzzy network Materials 2017, 10, 533 3 of 19 with an artificial bee colony and imperialist competitive algorithm for both forward and backward mapping of friction stir welded aluminum joints to maximize tensile strength, elongation, and hardness. Roshan et al. [26] employed adaptive neuro-fuzzy inference systems to determine the relationship between the main factors of the process, such as tool pin profile, tool rotary speed, welding speed, and axial force, and the main responses, including tensile strength, yield strength, and hardness of FSW aluminium 7075 plates. Then, the developed models were applied as an objective function to find the optimal process parameters using a simulated annealing algorithm. The main idea of this research was to study the joining of dissimilar materials AA6061 and AA7475 using the friction stir welding method. The objective of present work is to optimize the process parameters such as tool rotational speed, traverse speed and tilt angle for obtaining the greater or optimum value of mechanical properties like ultimate tensile strength, and micro-hardness of the friction stir welded joint of AA6061 and AA7475.

## 2. Materials and method

The workpieces joined by the FSW process are machined to the required dimensions. The required sizes of the plates are prepared based on the bed length and width of the milling machine, length of the backing plate, and the design of the clamping system so that the arrangements do not allow the distortion of plates due to forces induced by the rotating tool. However, the aluminum alloys are designed to be around 300 mm long and 80 mm wide sheet metal cut into the specified dimensions by a shear cutting technique. The final dimensions of the workpieces are 180 mm x 35 mm x 6.2 mm. The aluminum plates were machined at the sides to make them flat and ensure accurate face-to-face contact at the weld joint. This was accomplished using the shaping machine and a vice to hold the plates firmly. The experiments are developed by design expert

software. Three-factor and three-response surface design matrices were developed with 15 experiments. Mathematical modelling was carried out by response surface method (RSM), and optimum value was opting with RSM results. The chemical composition of the base plate and design of experiments is shown in table 1 and 2.

Table 1: Chemical composition of base material

Material	Si	Cu	Fe	Zn	Mg	Mn	Cr	Al
AA7475	0.15	0.84	0.12	5.24	1.96	0.045	0.14	Bal.
AA6061	0.85	0.21	0.65	0.3	0.85	0.11	0.2	Bal.

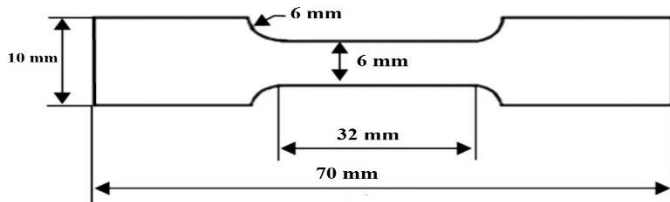


Figure 2: Dimension of tensile test specimen

The tensile stress of friction stir welded joints were measured under uniaxial tensile stress with the help of universal testing machine as per ASTM E8 standard as shown in fig. 2.

Table 2: Process parameters of friction stir welding

Sample No	A: TRS (rev/m)	B: T.S (mm/min)	C:Tilt Angle (°)
1	750	90	1
2	900	90	1
3	750	80	1
4	900	100	0
5	900	80	0
6	900	80	2
7	600	100	0
8	600	90	1
9	750	90	0
10	600	80	0
11	600	100	2
12	900	100	2
13	750	100	1
14	750	90	2
15	600	80	2

### 3. Results and discussion

#### 3.1 Tensile strength

Design expert software chose the processing parameters, TTA, TS, and TRS. Based on the input parameters, twenty experiments were carried out. The mechanical properties of AA6061 and AA7475 FSWed joints are examined below. Fig. 3 demonstrates the engineering stress strain of the welded joints and fig. 4 and 5 show the stress and % strain rose as the TRS increased. The UTS at the same TRS decreases as TS increases. The UTS value is smaller than the B.M; however, it is closer to the B.M at TRS 900 rev/m, TS 100 mm/min, and TTA 2°. According to the current findings a trade-off between UTS and microhardness should be addressed when selecting the ideal input values.

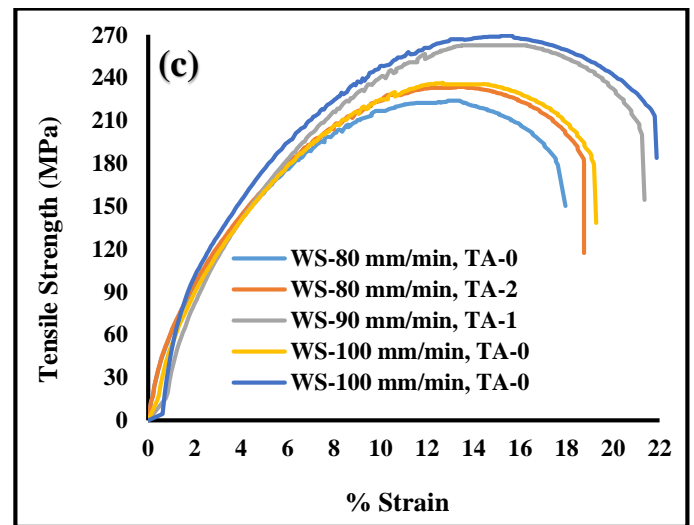
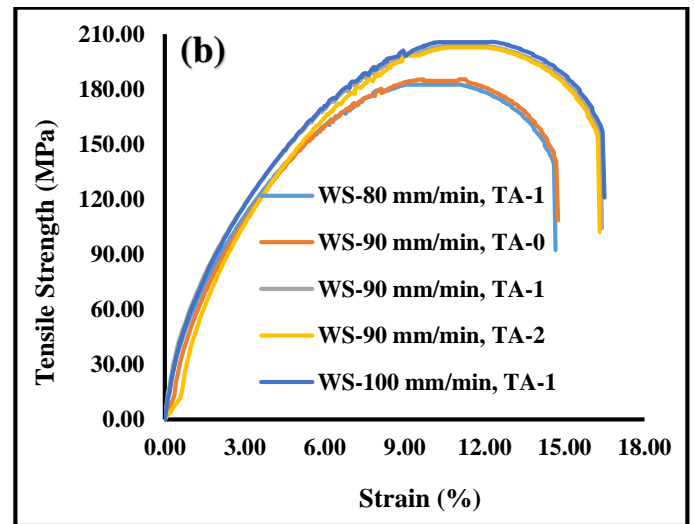
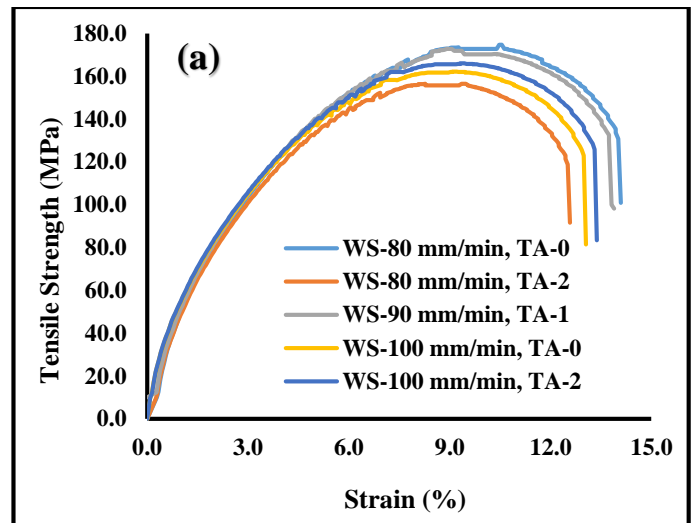


Figure 3: Stress strain diagram of welded joints of A6061 and AA7475, (a) 600 rpm, (b) 750 rpm, (c) 900 rpm

The heat input increases as the TRS increases, resulting in an ultrafine grain, which increases the UTS. While the TRS is faster

than 900 rev/m, it may generate too much heat on the B. M's top surface, causing a micro-void in the stir zone. The welded joint's UTS ranged from 155 to 270 MPa during all twenty experiments. At TS of 80 mm/min, TRS of 600 rev/m with tilt angle of 2°, the least UTS was perceived as 156.39 MPa, as shown in Fig. 4. The FSWed joint's UTS may be reduced if the temperature, grain coarsening, and cooling rate exceed the intended temperature. While material flows occurred on the A.S of the welded joint, some flaws were identified [27, 28]. All the tensile samples cracked on the advancing side HAZ and TMAZ area. This is likely due to numerous coarse grain brittle structures in TMAZ and HAZ areas [29, 30]. All the welded joints on the A.S failed, indicating that the UTS varies on both sides of the weld's center.

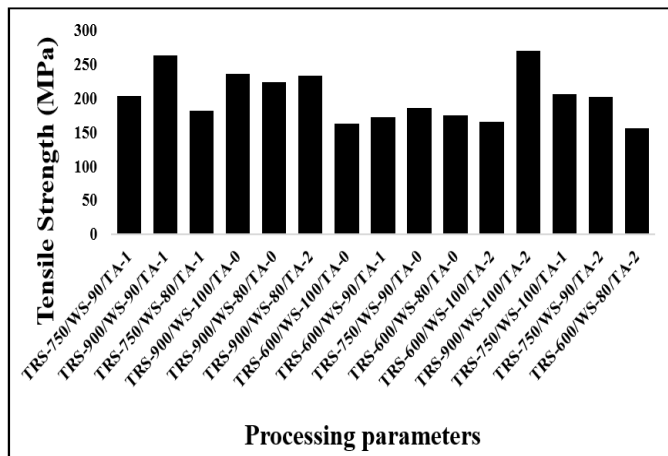


Figure 4: Variation of process parameters to the UTS.

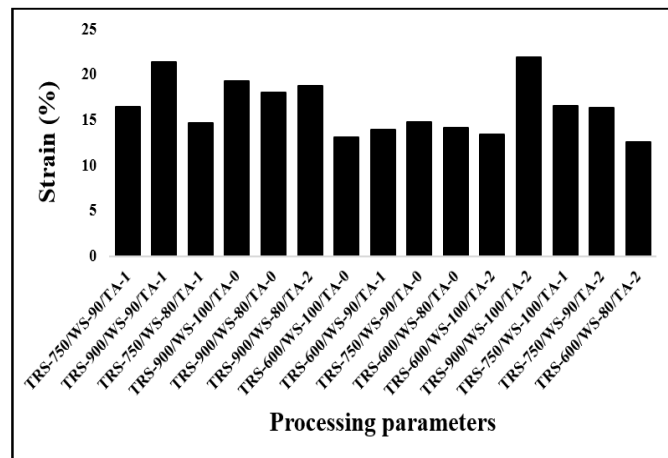


Figure 5: Variation of process parameters to the % strain

### 3.2 Hardness Measurement

The variation of process parameters and microhardness value of the FSWed joints of AA6061 and AA7475 is depicted in Fig. 6. The analysis of the micro-hardness across the weldment of AA6061 and AA7475, on the other hand, has been published previously [31]. The highest hardness was perceived in the SZ of the FSWed joint due to precipitation phase dissolution and fine recrystallized grain structure [32, 33]. The microhardness

value is pretentious by the grain structure, dislocation boundaries, and formation of precipitates. Because these regions had aging precipitates, coarse grain structure, and inadequate heat dispersion, the hardness value fell from the B.Ms to TMAZ and HAZ regions. The highest hardness of 103.45 HV was perceived TS of 90 mm-min<sup>-1</sup>, TRS of 900 rev/m, with tilt angle of 1°, whereas the lowest microhardness value of 61.51 HV was perceived at TRS of 600 rev/m, TS of 100 mm/min, and TTA of 0°.

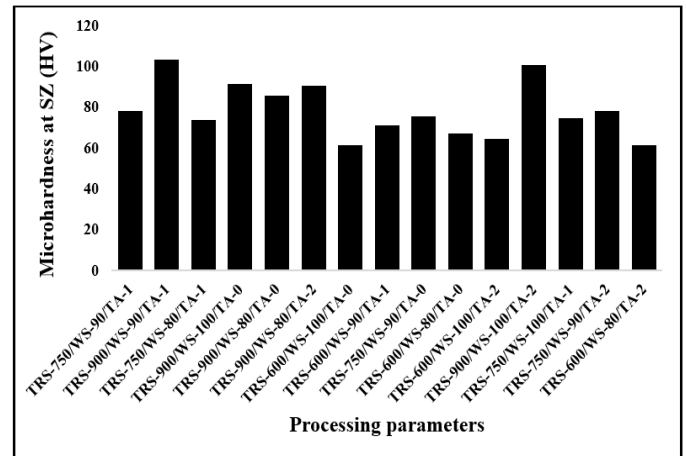


Figure 6: Variation of parameters and hardness at SZ

### 3.3 Estimating the adequacy of the developed model.

The response surface methodology (RSM) technique was used to assess the appropriateness of the empirical correlation for the output responses. Twenty experiments were carried out, all of which were planned using design expert software. The RSM technique used the ANOVA test to determine whether or not the input and output responses were statistically significant. Using the ANOVA approach, we can see which parameters influence the tensile characteristics of the welded joints of AA7475 and AA6061. We may conclude from the ANOVA test that the specified process parameters are essential in controlling the tensile strength of the FSWed joints [34, 35]. Tables 3-5 exhibit the ANOVA test findings for the output solutions. All models have a massively substantial Fisher's F value, revealing the model's adequacy. An expanded UTS model has a F-value of 63.58, indicating significant improvement. An F-value of the proposed model could occur owing to noise with a 0.01 percent error chance. The F-value for LOF was 1.72, indicating that the LOF is minor. The value of F should be insignificant in terms of the established model's appropriateness. Table 3 shows that the residual error value was 313.44, which has to be the total of the significance of P.E(115.05) and the value of LOF (198.39). A F-value of 59.40 was perceived for a developed model of percent strain, indicating that the produced model was significant. F-value of the proposed model would occur owing to noise with a 0.01 percent error chance. The F- value for LOF was 1.37, indicating that the LOF is minor. The value of F should be insignificant in terms of the established model's appropriateness. As shown in Table 4, the residual error value was observed to be 2.28, which should be the sum of P.E (0.9611) and the value of

LOF (1.32). A F-value of 70.42 was perceived for a developed model of hardness, indicating that the produced model was significant. F- value of the proposed model would occur owing to noise with a 0.01 percent error chance. The F-value for LOF

was 0.8269, indicating that the LOF is minor. The value of F should be insignificant in terms of the established model's appropriateness.

Table 3: ANOVA table for the UTS

Source	Sum of square	DOF	Mean of square	F Value	P Value	
<b>Model</b>	17935.93	9	1992.88	62.95	< 0.0001	Significant
A-TRS	15540.94	1	15540.94	495.81	< 0.0001	Significant
B-Traverse Speed	439.04	1	439.04	14.01	0.0038	Significant
C-TA	211.88	1	211.88	6.76	0.0265	Significant
AB	297.80	1	297.80	9.50	0.0116	Significant
AC	399.46	1	399.46	12.74	0.0051	Significant
BC	284.77	1	284.77	9.09	0.0130	Significant
A <sup>2</sup>	695.94	1	695.94	22.20	0.0008	Significant
B <sup>2</sup>	164.82	1	164.82	5.26	0.0448	Significant
C <sup>2</sup>	187.03	1	187.03	5.97	0.0347	Significant
<b>Residual</b>	313.44	10	31.34			
Lack of Fit (LOF)	198.39	5	39.68	1.72	0.2822	Not significant
Pure Error (P.E)	115.05	5	23.01			
<b>Cor Total</b>	18249.38	19				

Table 4: ANOVA table for the strain (%)

Source	Sum of square	DOF	Mean of square	F Value	P Value	
<b>Model</b>	121.86	9	13.54	59.40	< 0.0001	Significant
A-TRS	104.07	1	104.07	456.53	< 0.0001	Significant
B-Traverse Speed	3.62	1	3.62	15.90	0.0026	Significant
C-TA	1.43	1	1.43	6.27	0.0313	Significant
AB	2.75	1	2.75	12.06	0.0060	Significant
AC	2.63	1	2.63	11.55	0.0068	Significant
BC	1.65	1	1.65	7.23	0.0228	Significant
A <sup>2</sup>	5.47	1	5.47	24.01	0.0006	Significant
B <sup>2</sup>	1.09	1	1.09	4.77	0.0538	Significant
C <sup>2</sup>	1.23	1	1.23	5.40	0.0425	Significant
<b>Residual</b>	2.28	10	0.2280			
LOF	1.32	5	0.2637	1.37	0.3686	not significant
P.E	0.9611	5	0.1922			

Table 5: ANOVA table for the microhardness

Source	Sum of Squares	DOF	Mean of Square	F-value	p-value	
Model	2482.37	9	275.82	70.42	< 0.0001	Significant
A-TRS	2140.37	1	2140.37	546.48	< 0.0001	Significant
B-Traverse Speed	19.52	1	19.52	4.98	0.0497	Significant
C-TA	19.52	1	19.52	4.98	0.0497	Significant
AB	43.43	1	43.43	11.09	0.0076	Significant
AC	35.20	1	35.20	8.99	0.0134	Significant
BC	21.32	1	21.32	5.44	0.0418	Significant
A <sup>2</sup>	139.30	1	139.30	35.57	0.0001	Significant
B <sup>2</sup>	96.96	1	96.96	24.75	0.0006	Significant
C <sup>2</sup>	27.07	1	27.07	6.91	0.0252	Significant
Residual	39.17	10	3.92			
LOF	11.33	5	2.27	0.4069	0.8269	not significant
P.E	27.84	5	5.57			

### 3.4 Developed a mathematical model

The empirical relationship is developed for the output parameters under the following input variable.

$$UTS = 48.27 - 1.21A + 11.33B - 67.72C + 0.00418AB + 0.048AC + 0.58 BC + 0.00069A^2 - 0.0798 B^2 - 7.99C^2$$

$$\text{Strain (\%)} = 11.3 - 0.111A + 0.854B - 5.23C + 0.000391AB + 0.003825AC + 0.0453BC + 0.000063A^2 - 0.006291B^2 - 0.669C^2$$

$$\text{Hardness} = -183.42 - 0.5307A + 9.499B - 17.50C + 0.001553AB + 0.01398BC + 0.1632AC + 0.000316A^2 - 0.05937B^2 - 3.137C^2$$

### 3.5 Consequence of processing parameters on output values

The RSM method was implemented using design expert software to optimize process parameters and output responses. The generated model produces a 3D response graph and contour

plots using the optimal parameters. As demonstrated in figs. 7-9, input parameters impact the tensile characteristics of the weldment of AA6061 and AA7475. The red color indicates the high intensity peak, while the blue indicates the low intensity peak.

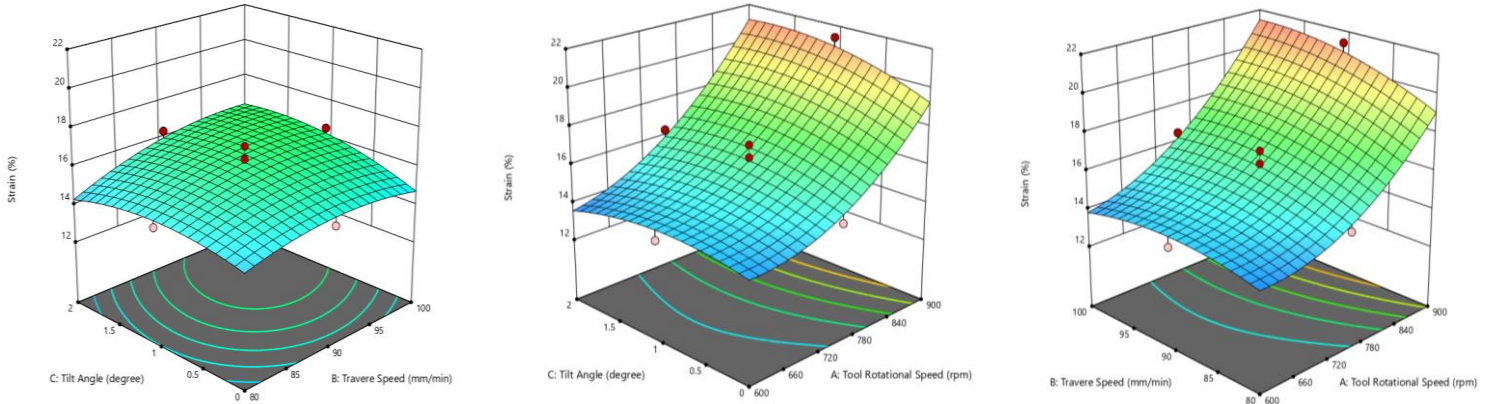


Figure 7: 3-D response surface diagram for Ultimate tensile strength

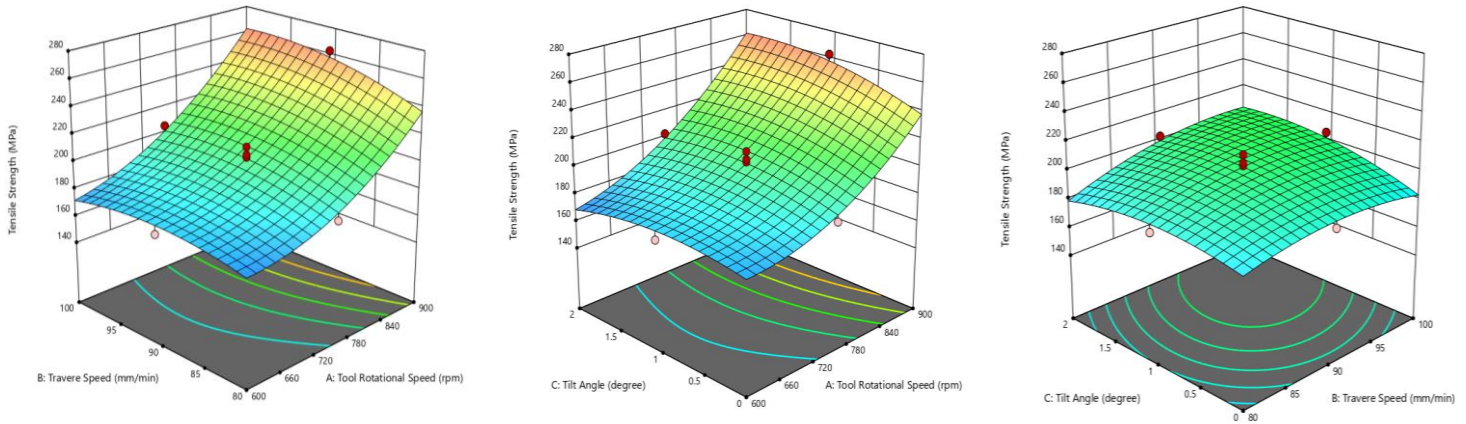


Figure 8: 3-D response surface diagram for % strain

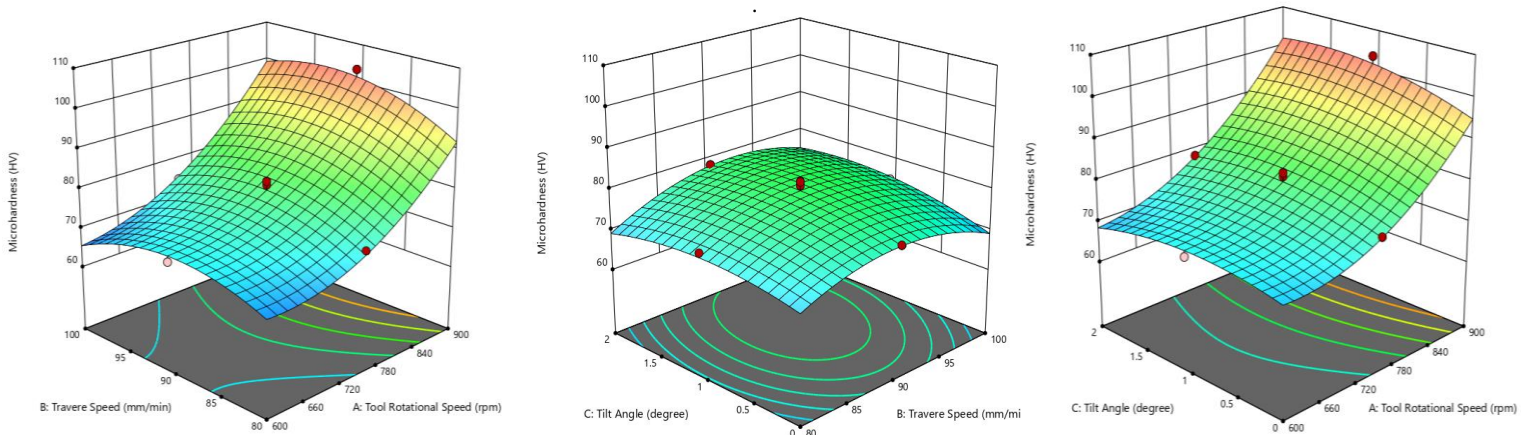


Figure 9: 3-D response surface diagram for hardness

When the TS increases, the UTS and hardness increase to a point; beyond that, these values fall as the temperature field changes, weakening the FSWed joints. UTS increases as TRS grows, but UTS increases at first and then declines when TTA increases, as seen in figs. 7 to 9.

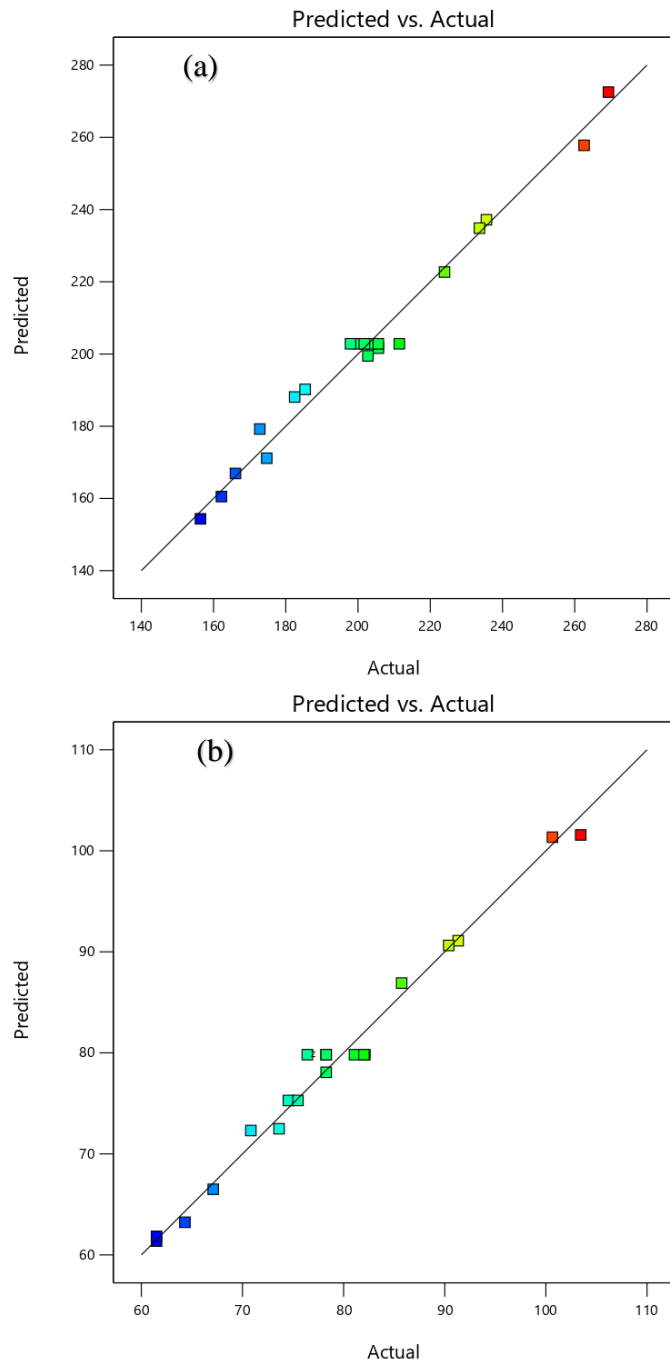


Figure 10: Predicted vs Actual Scatter diagram, (a) UTS (b) Hardness

The variation in output responses and input parameters of the FSWed joints of AA6061 and AA7475 is revealed in Fig. 7-9. The UTS increases as the TRS rises, whereas the UTS increases and decreases when the TS and TTA grow, because

substantial heat formation was detected at high TRS and low TS, the percent strain and hardness increased when the TRS increased, and when the TA and TS increased, the percent strain and microhardness increased first, then decreased. Fig. 10 shows the difference between the actual values and predicted values for output values and the built model's prediction capabilities. The errors were evenly spread through the model if the points were on a 45° straight line near the actual values. Fig. 10 shows a strong relationship between the generated model's predicted and actual values. The variation in output responses and input parameters of the FSWed joints of AA6061 and AA7475 is revealed in Fig. 7-9. The UTS increases as the TRS rises, whereas the UTS increases and decreases when the TS and TTA grow, because substantial heat formation was detected at high TRS and low TS, the percent strain and hardness increased when the TRS increased, and when the TA and TS increased, the percent strain and microhardness increased first, then decreased. Fig. 10 shows the difference between the actual values and predicted values for output values and the built model's prediction capabilities. The errors were evenly spread through the model if the points were on a 45° straight line near the actual values. Fig. 10 shows a strong relationship between the generated model's predicted and actual values. The multi-response optimization results are shown in Fig. 11. This method is used to optimize multiple objective functions at the same time. UTS, percent strain, and hardness at the SZ were optimized to 205.23 MPa, 16.43 %, and 81.05 HV, respectively, while TRS, feed rate, and TTA were tuned to 783.92 rev/m, 87.42 mm/min, and 0.48, respectively.

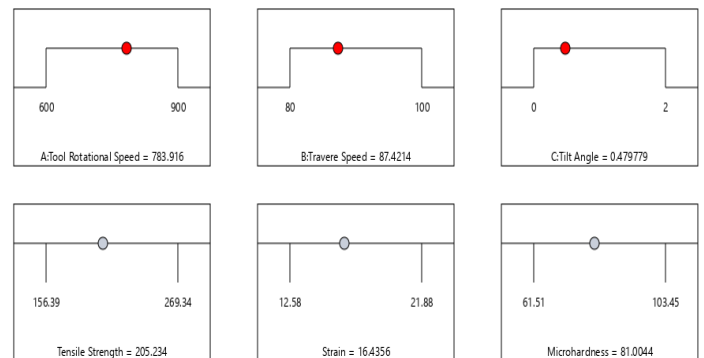


Figure 11: Ramp diagram for optimized value of input and output responses.

#### 4. Conclusions

The FSWed joint of AA6061 and AA7475 was successfully fabricated and perceived the following conclusions.

- The B.Ms (6.2 mm) of AA6061 and AA7475 were successfully fabricated via FSW. The experimentations were constructed using RSM's CCD and the input parameters, including TS, TRS, and TTA.
- The maximum UTS (269.34 MPa) was perceived at TRS of 900 rev/m, TS of 100 mm-min<sup>-1</sup> with a Tilt angle of 2°, while the minimum UTS (156.39 MPa) was perceived at

TS of 80 mm-min-1, TRS of 600 rev/m with a tilt angle of 2°.

- The highest microhardness (103.45 HV) was measured at TS of 90 mm-min-1, TRS of 900 rev/m with a tilt angle of 1°, whereas the least microhardness (61.51 HV) was measured at TS of 100 mm-min-1, TRS of 600 rev/m with a tilt angle of 0°.
- The empirical relationship between the output responses and input parameters was developed, and the perceived optimal values of UTS, percent strain, and microhardness at SZ were 205.23 MPa, 16.43 percent, and 81.05 HV, respectively. The optimal TS, TRS, and tilt angle values were 87.42 mm-min-1, 783.92 rev/m, and 0.48°, respectively.
- When the TRS and TS increase, the grain size decreases in the SZ. Furthermore, when the TRS is high, the temperature in the SZ rises. No common flaws were observed at high TRS of the welded joints of AA7475 and AA6061.

## References

- [1] Abdul Wahab Hashmi, Husain Mehdi, Sipokazi Mabuwa, Velaphi Msomi & Prabhujit Mohapatra, Influence of FSP Parameters on Wear and Microstructural Characterization of Dissimilar TIG Welded Joints with Si-rich Filler Metal. Silicon (2022). <https://doi.org/10.1007/s12633-022-01848-8>
- [2] Abdellah Nait Salah, Sipokazi Mabuwa, Husain Mehdi, Velaphi Msomi, Mohammed Kaddami, Prabhujit Mohapatra, Effect of Multipass FSP on Si-rich TIG Welded Joint of Dissimilar Aluminum Alloys AA8011-H14 and AA5083-H321: EBSD and Microstructural Evolutions. Silicon (2022). <https://doi.org/10.1007/s12633-022-01717-4>.
- [3] G. Buffa, J.Hua, R. Shivpuri, L. Fratini, A continuum based fem model for friction stir welding—model development, Materials Science and Engineering A 419 (2006) 389–396.
- [4] Cole, E.; Fehrenbacher, A.; Duffie, N.; Zinn, M.; Pfefferkorn, F.; Ferrier, N. Weld temperature effects during friction stir welding of dissimilar aluminum alloys 6061-t6 and 7075-t6. Int. J. Adv. Manuf. Technol. 2014, 71, 643–652.
- [5] RajKumar, V.; VenkateshKannan, M.; Sadeesh, P.; Arivazhagan, N.; Ramkumar, K.D. Studies on effect of tool design and welding parameters on the friction stir welding of dissimilar aluminium alloys AA 5052–AA 6061. Procedia Eng. 2014, 75, 93–97.
- [6] Guo, J.; Chen, H.; Sun, C.; Bi, G.; Sun, Z.; Wei, J. Friction stir welding of dissimilar materials between AA6061 and AA7075 Al alloys effects of process parameters. Mater. Des. 2014, 56, 185–192.
- [7] Mishra, R.S.; Mahoney, M.W. Friction Stir Welding and Processing; ASM International: Almere, The Netherlands, 2007.
- [8] Husain Mehdi, R.S. Mishra, Effect of Friction Stir Processing on Mechanical Properties and Wear Resistance of Tungsten Inert Gas Welded Joint of Dissimilar Aluminum Alloys. Journal of Materials Engineering and Performance volume, 30, 1926–1937 (2021). <https://doi.org/10.1007/s11665-021-05549-y>
- [9] Husain Mehdi, R.S. Mishra, Consequence of reinforced SiC particles on microstructural and mechanical properties of AA6061 surface composites by multi-pass FSP, Journal of Adhesion Science and Technology, 36(12), 1279-1298, 2022, <https://doi.org/10.1080/01694243.2021.1964846>.
- [10] Husain Mehdi, R.S. Mishra, Microstructure and mechanical characterization of tungsten inert gas-welded joint of AA6061 and AA7075 by friction stir processing, Proceedings of the Institution of Mechanical Engineers, Part L: Journal of Materials: Design and Applications, 235 (11), 2531-2546 (2021), <https://doi.org/10.1177/14644207211007882>.
- [11] Husain Mehdi, R.S. Mishra, Modification of Microstructure and Mechanical Properties of AA6082/ZrB2 Processed by Multipass Friction Stir Processing, Journal of Materials Engineering and Performance (2022). <https://doi.org/10.1007/s11665-022-07080-0>
- [12] Shojaeefard, M.H.; Behnagh, R.A.; Akbari, M.; Givi, M.K.B.; Farhani, F. Modelling and Pareto optimization of mechanical properties of friction stir welded AA7075/AA5083 butt joints using neural network and particle swarm algorithm. Mater. Des. 2013, 44, 190–198.
- [13] A. K. Lakshminarayanan, V. Balasubramanian, Trans. Nonferrous Met. Soc.China, 18(2008) 548-554.
- [14] Prakash Kumar Sahu, Sukhomay Pal, Journal of Magnesium and Alloys, 3 (2015) 36-46
- [15] C. Elanchezian, B. VijayaRammath, P. Venkatesan, S. Sathish, T. Vignesh, R.V. Siddharth, B. Vinay, K. Gopinath, Procedia Engineering, 97(2014) 775-782.
- [16] Husain Mehdi, R.S. Mishra (2016), Mechanical Properties and Microstructure Studies in Friction Stir Welding (FSW) Joints of Dissimilar Alloy-A Review, Journal of Achievements of Materials and Manufacturing Engineering , vol-77, issue1, pp 31-40.
- [17] Husain Mehdi, R.S. Mishra (2019), Analysis of Material Flow and Heat Transfer in Reverse Dual Rotation Friction Stir Welding: A Review, International Journal of Steel Structure, vol-19, issue-2, pp 422-434.
- [18] Husain Mehdi, R.S. Mishra (2019), Study of the influence of friction stir processing on tungsten inert gas welding of different aluminum alloy, SN Applied Sciences, vol-1, issue-7, 712.
- [19] Husain Mehdi, R.S. Mishra (2020), Investigation of mechanical properties and heat transfer of welded joint of AA6061 and AA7075 using TIG+FSP welding approach, Journal of Advanced Joining Processes, vol-1, issue-1, 100003.
- [20] Husain Mehdi, R.S. Mishra (2020), Effect of Friction Stir Processing on Microstructure and Mechanical Properties of TIG Welded Joint of AA6061 and AA7075, Metallography, Microstructure, and Analysis, vol-9, 403-418.
- [21] Husain Mehdi, R.S. Mishra, Effect of friction stir processing on mechanical properties and heat transfer of TIG welded joint of AA6061 and AA7075, Defence Technology, 17 (3), 715-727 (2021).
- [22] Husain Mehdi, R.S. Mishra (2020), Influence of friction stir processing on weld temperature distribution and mechanical properties of TIG welded joint of AA6061 and AA7075 Transactions of the Indian Institute of Metals, vol-73, 1773-1788.
- [23] Kasman, S. Multi-response optimization using the Taguchi-based grey relational analysis: A case study for dissimilar friction stir butt welding of AA6082-T6/AA5754-H111. Int. J. Adv. Manuf. Technol. 2013, 68, 795–804.
- [24] Rajakumar, S.; Balasubramanian, V. Multi-response optimization of friction-stir-welded AA1100 aluminum alloy joints. J. Mater. Eng. Perform. 2012, 21, 809–822.
- [25] Teimouri, R.; Baseri, H. Forward and backward predictions of the friction stir welding parameters using fuzzy-artificial bee colony-imprialist competitive algorithm systems. J. Intell. Manuf. 2012, 26, 307–319. [CrossRef]
- [26] Roshan, S.B.; Jooibari, M.B.; Teimouri, R.; Asgharzadeh-Ahmadi, G.; Falahati-Naghibi, M.; Sohrabpoor, H. Optimization of friction stir welding process of AA7075 aluminum alloy to achieve desirable mechanical properties using ANFIS models and simulated annealing algorithm. Int. J. Adv. Manuf. Technol. 2013, 69, 1803–1818.
- [27] A.Nait Salah, M. Kaddami, Husain Mehdi, Mechanical Properties And Microstructure Characterization of Friction Stir Welded Joint Of Dissimilar Aluminum Alloy AA2024 And AA7050, Turkish Journal of Computer and Mathematics Education, 12(7), 1051-1061 (2021).
- [28] M. Selvaraj , V. Murali , S. R. K. Rao , Mechanism of Weld Formation during Friction Stir Welding of Aluminum Alloy, Materials and Manufacturing Processes Volume 28 (5), 2013, 595-600.
- [29] Dharani Kumar S. Sendhil Kumar, Investigation of mechanical behavior of friction stir welded joints of AA6063 with AA5083 aluminum alloys, Mechanics and Mechanical Engineering 23(1), 2019, 59-63.
- [30] Abdul Wahab Hashmi, Husain Mehdi, R. S. Mishra, Prabhujit Mohapatra, Neeraj Kant & Ravi Kumar, Mechanical Properties and Microstructure Evolution of AA6082/Sic Nanocomposite Processed by Multi-Pass FSP. Transactions of the Indian Institute of Metals, (2022). <https://doi.org/10.1007/s12666-022-02582-w>.

- [31] Karthikeyan L, Senthil Kumar V S, Padmanabhan KA, On the role of process variables in the friction stir cast aluminum A319 alloy [J]. *Materials & Design*, 2010, 31(2): 761–771.
- [32] Azimzadegan T, Serajzadeh S. An Investigation into microstructures and mechanical properties of AA7075-T6 during friction stir welding at relatively high rotational speeds [J]. *Journal of Materials Engineering Performance*, 2010, 19(9): 1256–1263.
- [33] Husain Mehdi, Arshad Mehmood, Ajay Chinchkar, Abdul Wahab Hashmi, Chandrabhanu Malla, Prabhujit Mohapatra, Optimization of process parameters on the mechanical properties of AA6061/Al<sub>2</sub>O<sub>3</sub> nanocomposites fabricated by multi-pass friction stir processing, *Materials Today: Proceedings*, 56 (4), 1995-2003, 2021, <https://doi.org/10.1016/j.matpr.2021.11.3331>.
- [34] A.Nait Salaha, Husain Mehdi, Arshad Mehmood, Abdul Wahab Hashmid, Chandrabhanu Malla, Ravi Kumar, Optimization of process parameters of friction stir welded joints of dissimilar aluminum alloys AA3003 and AA6061 by RSM, *Materials Today: Proceedings*, 56 (4), 1675-1684, 2021, <https://doi.org/10.1016/j.matpr.2021.10.288>.
- [35] Husain Mehdi, R.S. Mishra, An experimental analysis and optimization of process parameters of AA6061 and AA7075 welded joint by TIG+FSP welding using RSM, *Advances in Materials and Processing Technologies*, 2020, <https://doi.org/10.1080/2374068X.2020.1829952>.

**Cite this article as:** Prashant Kumar, Sunil Kadyan, Rajesh Kumar, Optimization of process parameters of friction stir welded joint of dissimilar aluminum alloy by response surface methodology *International journal of research in engineering and innovation (IJREI)*, vol 6, issue 4 (2022), 236-244. <https://doi.org/10.36037/IJREI.2021.6405>